Regenerative Braking for EVs Using a Brushless DC Motor and Multi-Level Bidirectional Traction Converter

1st Fatemeh Nasr Esfahani
School of Engineering, Lancaster University
Lancaster, UK
f.nasresfahani@lancaster.ac.uk

2nd Javad Ebrahimi
Smith Engineering, Queen's University
Kingston, Canada
javad.ebrahimi@queensu.ca

3rd Alireza Bakhshai
Smith Engineering, Queen's University
Kingston, Canada
alireza.bakhshai@queensu.ca

4th Xiandong Ma
School of Engineering, Lancaster University
Lancaster, UK
xiandong.ma@lancaster.ac.uk

5th Ahmed Darwish
School of Engineering, University of Bradford
Bradford, UK
a.badawy4@bradford.ac.uk

***Abstract*- Brushless DC (BLDC) motors stand out as a preferred choice for electric vehicles (EVs) due to their high efficiency, precise speed control, and impressive torque-to-weight ratio. Regenerative braking, which recovers kinetic energy during deceleration, is crucial for enhancing EVs' driving range. This paper explores the development of a regenerative braking strategy for BLDC motors in EV applications. To establish the foundation for this strategy, a thorough examination of the dynamic model governing BLDC motors is conducted. The proposed regenerative braking strategy relies on accurately estimating the torque on the drive shaft by assessing various forces acting on an EV along an inclined road. A modular multilevel converter (MMC) equipped with two-stage isolated bidirectional SEPIC-full-bridge submodules (SMs) is used to manage power flow efficiently. Moreover, three-level space vector pulse width modulation (SVPWM) is implemented to increase the modulation index and reduce output total harmonic distortion (THD). The efficacy of the proposed regenerative braking strategy is validated by simulations across acceleration, constant speed, and deceleration modes.**

Keywords— Regenerative braking, Brushless DC motor, Electric vehicles, Multilevel multi-level converter

I. INTRODUCTION

With road transportation alone responsible for 27% of the UK's total greenhouse gas (GHG) emissions, it is evident that measures must be taken to mitigate environmental degradation [1]. Electric vehicles (EVs) emerge as a promising solution, offering the potential to substantially reduce GHG emissions and decrease gasoline consumption [2-4].

EV technology revolves around essential components, such as the high voltage (HV) battery pack, low voltage (LV) battery system, traction converter, electric motor, battery charger, etc. [5-7]. Among these components, the choice of electric motor is crucial. While traditional DC motors were once prevalent, they suffer from drawbacks like high maintenance, low power density, and low efficiency [8]. In contrast, induction motors (IMs), switched reluctance machines (SRMs), permanent magnet synchronous machines (PMSMs), and brushless DC (BLDC) machines offer superior performance, with BLDC motors standing out for their efficiency, power density, and torque-to-weight ratio advantages [9].

The traction converter also plays a vital role in the EV propulsion system [10]. Multi-level converters such as neutral point clamped (NPC), flying capacitor (FC), cascaded half-bridge (CHB), and modular multilevel converters (MMCs) with several benefits, including lower total harmonic distortion (THD), higher efficiency, and reduced stress on semiconductor devices are widely used as traction converter or battery chargers in EV applications [11-14].

EVs still suffer from challenges like limited driving and battery ranges, highlighting the importance of regenerative braking systems [15]. Recent research has focused on optimizing regenerative braking systems for BLDC motors in EVs, with various strategies proposed to enhance energy recovery efficiency [16-18]. Supercapacitors and ultracapacitors have also shown promise in improving energy recovery compared to conventional batteries, offering a more efficient solution for storing regenerated energy [17].

This paper proposes a regenerative braking strategy, supported by an MMC and a proper SVPWM modulation, to enhance the performance of the BLDC motor. This paper presents a thorough solution that enhances the overall performance of EVs. The proposed approach not only seeks to improve the efficiency of regenerative braking systems but also to extend the driving range of EVs, making them more practical and appealing to consumers.

The rest of this paper is organized as follows: Section II outlines the dynamic modelling of the BLDC motor. Section III presents the dynamic modelling of the EV to estimate drive shaft's torque. Section IV delves into the details of the proposed regenerative braking strategy. Section V discusses the modular multilevel traction converter and the employed modulation technique. Simulation results are provided in Section VI. Finally, conclusions are drawn in Section VII.

II. BLDC DYNAMIC MODELLING

BLDC motors offer several advantages including a high power-to-weight ratio, high speed capabilities, precise control of speed (rpm) and torque, high efficiency, and low maintenance requirements. To derive the dynamic model of a BLDC motor, the three-phase voltages applied to the stator windings are expressed as [9]:

$$\begin{cases} v_a(t) = r_s i_a + e_a \\ v_b(t) = r_s i_b + e_b \\ v_c(t) = r_s i_c + e_c \end{cases} \tag{1}$$

, with r_s and e_i (i=a, b, c) being the stator winding resistance and three-phase back emfs, respectively. The back emfs e_i are equal to flux variations over a given time and can be calculated as (2), with L_i (i=a, b, c) being the inductance of the BLDC motor per phase. M_{xy} (x, y=a, b, c) is the mutual inductance between different phases.

$$\begin{cases} e_a = \dfrac{d\psi_a}{dt} = \dfrac{d}{dt}(L_a i_a + M_{ab} i_b + M_{ac} i_c + \psi_{pm}(\theta_e)) \\ e_b = \dfrac{d\psi_b}{dt} = \dfrac{d}{dt}(L_b i_b + M_{ba} i_a + M_{bc} i_c + \psi_{pm}(\theta_e)) \\ e_c = \dfrac{d\psi_c}{dt} = \dfrac{d}{dt}(L_c i_c + M_{cb} i_b + M_{ca} i_a + \psi_{pm}(\theta_e)) \end{cases} \quad (2)$$

$\psi_{pm}(\theta_e)$ indicates the flux linkage due to the rotor magnets linking the stator as:

$$\psi_{pm}(\theta_e) = N\varphi_{pm}(\theta_e) = N\int_{-\frac{\pi}{2}+\theta_e}^{\frac{\pi}{2}+\theta_e} AB(\theta_e')d\theta_e' \quad (3)$$

, where N, A, B, and θ_e are the number of turns per phase, the rotor area, the permanent magnet flux density of the rotor, and the electrical angle of the rotor. To simplify the equations, it is assumed that the three-phase stator windings are symmetrical, so the self and mutual inductance of all phases are equal and constant, as shown in (4). Therefore, (2) can be rewritten as (5) and can be simplified as (6).

$$\begin{cases} L_a = L_b = L_c = L \\ M_{ab} = M_{ba} = M_{ac} = M_{ca} = M_{bc} = M_{cb} = M \end{cases} \quad (4)$$

$$\begin{cases} e_a = L\dfrac{di_a}{dt} + M(\dfrac{di_b}{dt} + \dfrac{di_c}{dt}) + \dfrac{d}{dt}(\psi_{pm}(\theta_e)) \\ e_b = L\dfrac{di_b}{dt} + M(\dfrac{di_a}{dt} + \dfrac{di_c}{dt}) + \dfrac{d}{dt}(\psi_{pm}(\theta_e)) \\ e_c = L\dfrac{di_c}{dt} + M(\dfrac{di_b}{dt} + \dfrac{di_a}{dt}) + \dfrac{d}{dt}(\psi_{pm}(\theta_e)) \end{cases} \quad (5)$$

$$\begin{cases} e_a = L\dfrac{di_a}{dt} + M(\dfrac{di_b}{dt} + \dfrac{di_c}{dt}) + E_a \\ e_b = L\dfrac{di_b}{dt} + M(\dfrac{di_a}{dt} + \dfrac{di_c}{dt}) + E_b \\ e_c = L\dfrac{di_c}{dt} + M(\dfrac{di_b}{dt} + \dfrac{di_a}{dt}) + E_c \end{cases} \quad (6)$$

, in which:

$$\begin{cases} E_a = \omega_e \psi_m f_a(\theta_e) \\ E_b = \omega_e \psi_m f_b(\theta_e) = f_a(\theta_e - \dfrac{2\pi}{3}) \\ E_c = \omega_e \psi_m f_c(\theta_e) = f_a(\theta_e + \dfrac{2\pi}{3}) \end{cases} \quad (7)$$

, where ψ_m is the maximum flux linkage, ω_e is the electrical velocity, and $f(\theta_e)$ represents the back-emf reference.

Finally, the three-phase voltages can be re-written as:

$$\begin{cases} v_a(t) = r_s i_a + L\dfrac{di_a}{dt} + M(\dfrac{di_b}{dt} + \dfrac{di_c}{dt}) + E_a \\ v_b(t) = r_s i_b + L\dfrac{di_b}{dt} + M(\dfrac{di_a}{dt} + \dfrac{di_c}{dt}) + E_b \\ v_c(t) = r_s i_c + L\dfrac{di_c}{dt} + M(\dfrac{di_b}{dt} + \dfrac{di_a}{dt}) + E_c \end{cases} \quad (8)$$

The torque equation for the BLDC motor is given by:

$$T_{em} - T_L = B\omega_m + J\frac{d\omega_m}{dt} \quad (9)$$

, with ω_m being the mechanical velocity. The relation between the electrical velocity ω_e, mechanical velocity ω_m, and the electrical angle of the rotor θ_e can be expressed as (10), with P being the number of rotor poles:

$$\begin{cases} \omega_e = \dfrac{P}{2}\omega_m \\ \theta_e = \int \omega_e(t)dt \end{cases} \quad (10)$$

The electromagnetic torque is expressed as:

$$T_{em} = \psi_m(f_a(\theta_e)i_a + f_b(\theta_e)i_b + f_c(\theta_e)i_c) \quad (11)$$

III. EV DYNAMIC MODELING

The velocity profile depicting an EV along an inclined road is illustrated in Fig. 1. The total force F_{te} demanded by the EV encompasses the hill-climbing force F_{hc}, the friction force F_{rr}, the aerodynamic force F_{ad}, and the acceleration force F_{la}, represented as (12), where the forces are defined as (13).

$$F_{te} = F_{rr} + F_{hc} + F_{ad} + 1.05F_{la} \quad (12)$$

$$\begin{cases} F_{rr} = \mu_{rr} mg \\ F_{hc} = mg\sin(\delta) \\ F_{ad} = \dfrac{1}{2}\rho S C_d v^2 \\ F_{la} = ma \end{cases} \quad (13)$$

, where μ_{rr} represents the rolling resistance coefficient, δ denotes the inclination of the road surface, g signifies the acceleration due to gravity, and ρ stands for the density of air. Additionally, v, a, S, C_d, and m correspond to velocity, acceleration, frontal area, drag coefficient, and vehicle mass, respectively.

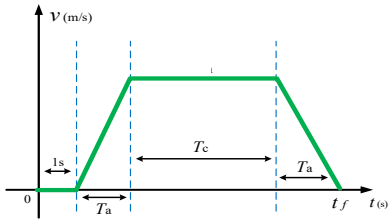

Fig. 1. Velocity profile of EV along an inclined road

Torque at the wheel side T_w can be calculated as the product of the force applied and the wheel radius r. Additionally, considering the presence of a gearbox with the gear ratio G between the motor and the wheel, the mechanical speed at the motor side ω_m equals $G.\omega_w$, with ω_w being speed the speed at the wheel side. Finally, the required shaft torque at the motor side T_m can be calculated as:

$$\begin{aligned} T_m &= \frac{mgr(\mu_{rr} + \sin(\delta))}{G} + \frac{1}{2G^3}\rho S C_d \omega_m^2 r^3 + \frac{1.05 m r^2 \alpha_m}{G^2} \\ &= T_F + K_d\omega_m^2 + J_m\alpha_m \end{aligned} \quad (14)$$

, with α_m being the acceleration.

IV. REGENERATIVE BRAKING APPLIED TO BLDC MOTOR

During braking, a significant portion of kinetic energy is dissipated as heat and released into the environment, resulting in energy wastage. However, EVs equipped with regenerative braking systems can capture this kinetic energy, convert it into electricity, and store it for later use. This capability extends both the battery life and the driving range of the EV. The typical configuration of an EV equipped with acceleration

(driving mode) and regenerative braking (deceleration) modes is depicted in Fig. 2. In this figure, red and blue arrows symbolize the power flow during "acceleration" and "deceleration", respectively.

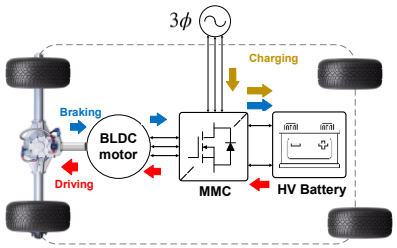

Fig. 2. Power flow in driving, charging and regenerative braking modes

From the EV dynamic modelling discussed in the previous section, the required drive shaft torque T_L can be calculated using (15), where the constants T_F and K_d are defined as (16):

$$T_L = T_F + K_d \omega_m^2 \tag{15}$$

$$\begin{cases} T_F = \dfrac{\mu_{rr} mgr}{G} \\ K_d = \dfrac{1}{2G^3} \rho A C_d r^3 \end{cases} \tag{16}$$

The currents at the input and output terminals of a BLDC motor are equal, so $i_a+i_b+i_c=0$. Also, in BLDC motors, only two phases conduct at a time t. For $i_c=0$, we can have:

$$i_a = -i_b \tag{17}$$

Therefore, (11) can be re-written as:

$$T_{em_{ref}} = \psi_m (f_a(\theta_e) i_a - f_b(\theta_e) i_a) = \psi_m i_a (f_a(\theta_e) - f_b(\theta_e)) \tag{18}$$

, and from there, the reference value of the phase-*a* current $i_{a_{ref}}$ and three-phase voltage equations can be extracted as (19) and (20), respectively:

$$i_{a_{ref}} = \frac{T_{em_{ref}}}{\psi_m (f_a(\theta_e) - f_b(\theta_e))} \tag{19}$$

$$\begin{cases} v_{a_{ref}}(t) = r_s i_{a_{ref}} + L \dfrac{di_{a_{ref}}}{dt} - M \dfrac{di_{a_{ref}}}{dt} + E_a \\ v_{b_{ref}}(t) = -r_s i_{a_{ref}} - L \dfrac{di_{a_{ref}}}{dt} + M \dfrac{di_{a_{ref}}}{dt} + E_b \\ v_{c_{ref}}(t) = E_c \end{cases} \tag{20}$$

The block diagram of implementing regenerative braking using the BLDC is shown in Fig. 3. As can be seen, firstly, the reference velocity profile V^* is used to generate the reliable value of drive shaft torque T_L. Next, the reference value of the electromagnetic torque $T_{em_{ref}}$ can be calculated from (9). Then, (19) and (20) are used to extract the reference value of the phase-*a* current $i_{a_{ref}}$ and three-phase voltages v_{aref}, v_{bref}, and v_{cref} to be applied to the stator windings. Here, a three-level converter with two-stage SMs is used as the bidirectional traction converter. More details on the traction converter and its modulation are presented in the next section.

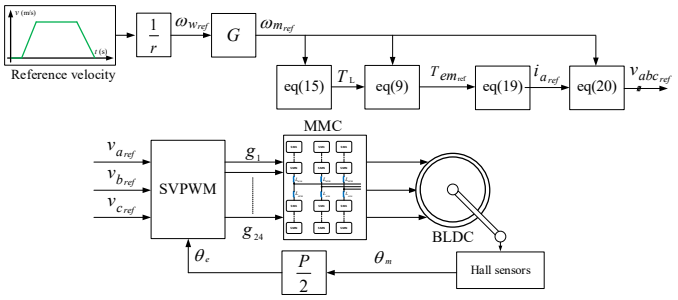

Fig. 3. The proposed regenerative braking strategy using BLDC

V. Modular Three-Level Traction Converter

A. MMC topology

Fig. 4 illustrates the three-phase configuration of the modular topology employed as the integrated traction inverter. An isolated bidirectional Single-Ended Primary Inductance Converter (SEPIC) converter is utilized on the battery side in this setup. The SEPIC converter draws a constant current from the battery (due to its input inductor), while its output capacitor filters the output voltage for subsequent stages. Featuring an embedded High-Frequency Transformer (HFT), the SEPIC converter provides a form of galvanic isolation between the battery pack and the motor or utility grid. Subsequently, the SEPIC converter is connected to a full-bridge converter to produce the required AC voltage at the motor terminals.

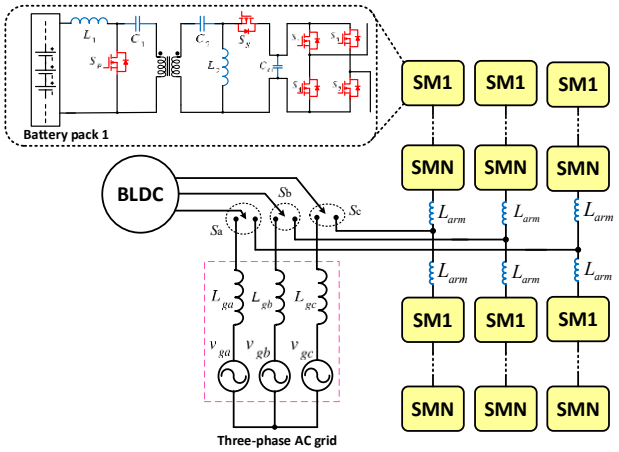

Fig. 4. The three-phase layout of the MMC topology

The two-stage converter SM facilitates bidirectional power flow during various modes of operation:

1. Normal driving (discharging): power flows from batteries to the electric motor.
2. Regenerative braking: converting kinetic energy to electricity and storing it in the batteries.
3. Charging: power flows from the AC grid to the batteries

B. Three-level space vector pulse width modulation

By employing an appropriate modulation technique, the power rating of the MMC topology can be enhanced to meet the requirements of EV charging infrastructures. Sinusoidal pulse-width modulation (SPWM) is a commonly used technique in power electronics applications. However, it has

been observed to result in higher THD in the output voltages when SPWM is utilized [19]. In contrast, Space Vector Pulse Width Modulation (SVPWM) has been demonstrated to generate a more efficient output voltage with a higher modulation index and lower THD [20-21]. This modulation technique yields an output voltage approximately 15% higher than conventional modulation methods, leading to a more efficient utilization of the input DC power supply.

The space vector diagram for the three-level inverter is divided into six sectors with a 60° phase difference, as shown in Fig. 5(a). The Clark transformation is used to transfer the three-phase AC voltages to the stationary reference frame α-β. Then, the resulting V_α and V_β are used to extract the magnitude V_{ref} and angle θ (in radians) of the rotating vector.

$$v_{abc} = V_m \left[\sin(\omega t) \quad \sin(\omega t - \frac{2\pi}{3}) \quad \sin(\omega t - \frac{4\pi}{3}) \right]^T \tag{21}$$

$$\begin{bmatrix} V_\alpha \\ V_\beta \end{bmatrix} = \sqrt{\frac{2}{3}} \begin{bmatrix} 1 & -0.5 & -0.5 \\ 0 & \frac{\sqrt{3}}{2} & -\frac{\sqrt{3}}{2} \end{bmatrix} \begin{bmatrix} v_a \\ v_b \\ v_c \end{bmatrix} \tag{22}$$

$$|V_{ref}| = \sqrt{V_\alpha^2 + V_\beta^2} \tag{23}$$

$$\theta = \tan^{-1}(\frac{V_\beta}{V_\alpha}) \tag{24}$$

V_{ref} can be found with two adjacent active vectors and one zero vector. The time duration of the associated vectors (sectors' duration) is as follows:

$$T_1 = \sqrt{3} T_s \frac{V_{ref}}{V_{in}} \sin(k\frac{\pi}{3} - \theta) \tag{25}$$

$$T_2 = \sqrt{3} T_s \frac{V_{ref}}{V_{in}} \sin(\theta - \frac{(k-1)\pi}{3}) \tag{26}$$

$$T_0 = T_s - (T_1 + T_2) \tag{27}$$

, where T_s and V_{in} are the total cycle and the DC input voltage, respectively. The factor k=1,…,6 also represents the sector number. The three-level converter is characterized by 3^3= 27 switching states with 24 active states and three zero states that lie at the centre of the hexagon, and each sector has four regions. Region selection depends on the Modulation Index m_{n}, m_1, and m_2:

$$m_n = \frac{V_{ref}}{\frac{2}{3} V_{in}} \tag{28}$$

$$m_1 = m_n(\cos(\alpha) - \frac{\sin(\alpha)}{\sqrt{3}}) \tag{29}$$

$$m_2 = \frac{2}{\sqrt{3}} m_n \sin(\alpha) \tag{30}$$

If the value of m_1, m_2, and $(m_1+m_2) < 0.5$, then V_{ref} lies in region 1, as shown in Fig.5(b). If the value of m_1 and $m_2 < 0.5$ and $(m_1+m_2) > 0.5$, then V_{ref} lies in region 2. If the valve of $m_1 > 0.5$, then V_{ref} lies in region 3. If the value of $m_2 > 0.5$, then V_{ref} lies in region 4. The switching times for Sector 1 are listed are Table I. As an example, if V_{ref} is in region 2, it can be composed by voltage vectors V_1, V_2, and V_8 as shown in Fig. 5(c). Therefore, the equations of ON-time of the voltage vectors can be given as:

$$V_{ref} \cdot T_s = V_1 \cdot t_a + V_8 \cdot t_b + V_2 \cdot t_c \tag{31}$$

, where $T_s = t_a + t_b + t_c$

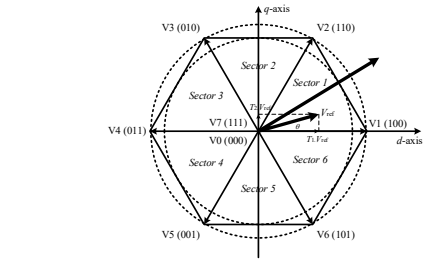

Fig. 5. Space vector diagram for a three-level inverter demonstrating (a) voltage space vector (b) sub-regions of Sector 1 (c) switching vectors and times in Sector 1

Table I. Switching times for Sector 1

Region	t_a	t_b	t_c
1	$\frac{4}{\sqrt{3}} m_n T_s \sin(\frac{\pi}{3} - \alpha)$	$T_s - \frac{4}{\sqrt{3}} m_n T_s \sin(\frac{\pi}{3} + \alpha)$	$\frac{4}{\sqrt{3}} m_n T_s \sin(\alpha)$
2	$T_s - \frac{4}{\sqrt{3}} m_n T_s \sin(\alpha)$	$\frac{4}{\sqrt{3}} m_n T_s \sin(\frac{\pi}{3} + \alpha) - T_s$	$T_s - \frac{4}{\sqrt{3}} m_n T_s \sin(\frac{\pi}{3} - \alpha)$
3	$2T_s - \frac{4}{\sqrt{3}} m_n T_s \sin(\frac{\pi}{3} + \alpha)$	$\frac{4}{\sqrt{3}} m_n T_s \sin(\alpha)$	$\frac{4}{\sqrt{3}} m_n T_s \sin(\frac{\pi}{3} - \alpha) - T_s$
4	$\frac{4}{\sqrt{3}} m_n T_s \sin(\alpha) - T_s$	$\frac{4}{\sqrt{3}} m_n T_s \sin(\frac{\pi}{3} - \alpha)$	$2T_s - \frac{4}{\sqrt{3}} m_n T_s \sin(\frac{\pi}{3} + \alpha)$

VI. Simulation Results

With the BLDC machine's parameters listed in Table II, simulation results for the 5-level phase-to-phase and 3-level phase-to-ground voltages are depicted in Fig. 6(a) and (b) respectively.

Table II. BLDC machine parameters

Parameter	Value
Stator resistance (per phase)	0.02Ω
Stator inductance (per phase)	2.1 mH
Number of poles	4
Back emf coefficient	0.098 V/(rad/sec)
Moment of inertia	0.309 kg.m^2

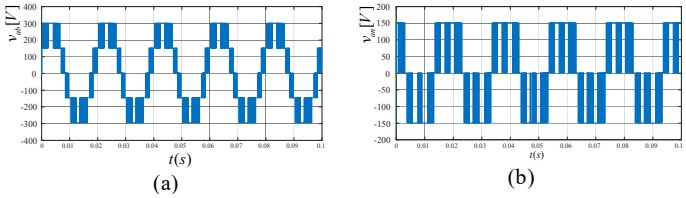

Fig. 6. Simulation results (a) five-level phase-to-phase voltage v_{ab} (b) three-level phase-to-ground voltage in phase *a*

Fig. 7(a)-(d) illustrates the simulation results for the rotor speed ω_{m}, electromagnetic torque T_{e}, stator current (phase a),

and input current I_{in} (battery current). The actual rotor speed ω_m in red closely tracks its reference value in blue across various operating modes, including zero speed, acceleration, constant speed, and deceleration. The electromagnetic torque T_e initially remains at zero for the first second when the rotor speed ω_m is zero, indicating that the EV is stationary. As acceleration occurs, the torque gradually increases. During constant speed operation, the torque remains steady but at a lower level compared to the acceleration phase, indicating that the EV is maintaining its speed without additional acceleration. During deceleration, the electromagnetic torque T_e becomes negative, signifying the reversal of torque direction as the EV slows down. The battery current I_{in} exhibits an increasing trend after regenerative braking, indicating the transfer of energy from the motor to the batteries. This behaviour aligns with the concept of regenerative braking.

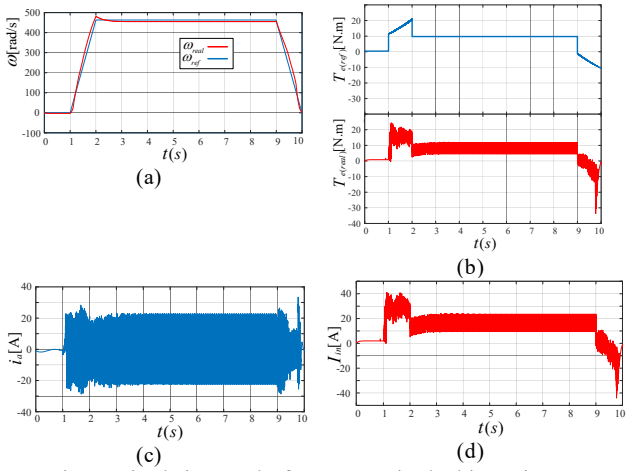

Fig. 7. Simulation results for regenerative braking using BLDC: (a) Rotor speed ω_m(rad/s) (b) Electromagnetic torque T_e (N.m) (c) stator current i_a (d) Input current I_{in} (Battery current)

VII. Conclusion

A straightforward regenerative braking strategy, featuring BLDC motors is presented in This paper. At the heart of this study lies the dynamic modelling of BLDC motors, which is a fundamental step in understanding their behaviour and performance characteristics. Through meticulous analysis of the forces along an inclined road, the drive shaft torque is estimated which is a crucial parameter in the regenerative braking strategy. A key aspect here is the implementation of the SVPWM technique to generate three-phase stator winding voltages, increasing the modulation index and lowering THD. The performance of the proposed strategy is validated across all operational modes, including acceleration, deceleration, and constant speed, through simulations. From the simulation results, the battery current exhibits a rising trend after regeneration at braking, indicating the transfer of energy from the motor to the batteries.

References

[1] F. Nasr Esfahani, A. Darwish, and B. W. Williams, "Power converter topologies for grid-tied solar photovoltaic (PV) powered electric vehicles (EVs)-A comprehensive review," *Energies*, vol. 15, no. 13, pp. 4648, 2022.

[2] M. Niroomand, F. Nasr Esfahani, S. M. Tripathi, and S. Padmanaban, "Converter technologies for PV systems: A comprehensive review," *Energy Conversion Systems: An Overview*, pp. 1-58, 2021.

[3] M. Niroomand, F. Nasr Esfahani, S. M. Tripathi, and S. Padmanaban, "Control Structures of Grid-Tied Photovoltaic Systems," pp. 59-133, 2021.

[4] F. Nasr Esfahani, A. Darwish, and A. Massoud, "PV/battery grid integration using a modular multilevel isolated SEPIC-based converter," Energies, vol. 15, no. 15, pp. 5462, 2022.

[5] J. Ebrahimi, O. Salari, S. Eren, K. Hashtrudi-Zaad, A. Bakhshai and P. Jain, "Efficiency Improved Multi-Source Inverter for Hybrid Energy Storage Systems in Electric Vehicle Application," *IEEE Transactions on Power Electronics*, vol. 37, no. 2, pp. 1982-1997, Feb. 2022.

[6] J. Ebrahimi and S. Eren, "A Multi-Source DC/AC Converter for Integrated Hybrid Energy Storage Systems," *IEEE Transactions on Energy Conversion*, vol. 37, no. 4, pp. 2298-2309, Dec. 2022.

[7] F. Nasr Esfahani, A. Darwish, and X. Ma, "Design and Control of a Modular Integrated On-Board Battery Charger for EV Applications with Cell Balancing," *Batteries*, vol. 10, no. 1, pp. 17, 2024.

[8] A. Karki, S. Phuyal, D. Tuladhar, S. Basnet, and B. P. Shrestha, "Status of pure electric vehicle power train technology and future prospects," *Applied System Innovation*, vol. 3, no. 3, p. 35, 2020.

[9] R. Krishnan, "Permanent magnet synchronous and brushless DC motor drives. *CRC press*, 2017.

[10] F. Nasr Esfahani, A. Darwish, X. Ma, and P. Twigg, "Non-Integrated and Integrated On-Board Battery Chargers (iOBCs) for Electric Vehicles (EVs): A Critical Review," *Energies*, vol. 17, no. 10, pp. 2285, 2024.

[11] J. Ebrahimi and H. Karshenas, "N-Tuple Flying Capacitor Multicell Converter-A Generalized Modular Hybrid Topology," *IEEE Transactions on Industrial Electronics*, vol. 66, no. 7, pp. 5004-5014, July 2019.

[12] J. Ebrahimi, H. Karshenas, S. Eren and A. Bakhshai, "An Optimized Capacitor Voltage Balancing Control for a Five-Level Nested Neutral Point Clamped Converter," *IEEE Transactions on Power Electronics*, vol. 36, no. 2, pp. 2154-2165, Feb. 2021.

[13] J. Ebrahimi, H. Karshenas and A. Bakhshai, "A Five-Level Nested Diode-Clamped Converter for Medium-Voltage Applications," in IEEE Transactions on Industrial Electronics, vol. 69, no. 7, pp. 6471-6483, July 2022.

[14] J. Ebrahimi and H. Karshenas, "A New Single DC Source Six-Level Flying Capacitor Based Converter with Wide Operating Range," *IEEE Transactions on Power Electronics*, vol. 34, no. 3, pp. 2149-2158, March 2019.

[15] F. Nasr Esfahani, and A. Darwish, "Regenerative Braking for EVs Using PMSM with CHB as Bidirectional Traction Converter," In *2022 IEEE 16th International Conference on Compatibility, Power Electronics, and Power Engineering (CPE-POWERENG)*, pp. 1-7. IEEE, 2022.

[16] A. K. Mishra, A. K. Singh, and G. M. Vishwanath, "A Fuel-Efficient BLDC Motor-Driven Light Electric Vehicle with Single-Stage Onboard Charging System," in *IEEE Transactions on Transportation Electrification*, vol. 9, no. 4, pp. 4909-4921, Dec. 2023

[17] I. Shchur and V. Turkovskyi, "Multilevel DC Link Inverter Fed BLDC Motor Drive with Modular Battery/Supercapacitor HESS for Electric Vehicle," *2020 IEEE Problems of Automated Electrodrive. Theory and Practice (PAEP)*, Kremenchuk, Ukraine, 2020, pp. 1-6

[18] S. S. Pasupuleti, N. R. Tummuru and H. Misra, "Power Management of Hybrid Energy Storage System Based Wireless Charging System with Regenerative Braking Capability," in *IEEE Transactions on Industry Applications*, vol. 59, no. 3, pp. 3785-3794, May-June 2023

[19] J. Ebrahimi, H. Karshenas, S. Eren, and A. Bakhshai, "A Fast-Decoupled Space Vector Modulation Scheme for Flying Capacitor-Based Multilevel Converters," *IEEE Transactions on Power Electronics*, vol. 36, no. 12, pp. 14539-14549, Dec. 2021.

[20] J. Ebrahimi, S. Shahnooshi, S. Eren, H. Karshenas and A. Bakhshai, "Optimized Switching Frequency Voltage Balancing Schemes for Flying Capacitor Based Multilevel Converters," *IEEE Transactions on Industrial Electronics*, vol. 70, no. 11, pp. 10775-10788, Nov. 2023.

[21] J. Ebrahimi, S. Shahnooshi, S. Eren and A. Bakhshai, "A Modulation Scheme Based on Virtual Voltage Levels for Capacitor Voltage Balancing of the Four-Level Diode Clamped Converter," *IEEE Transactions on Power Electronics*, vol. 38, no. 4, pp. 4727-4744, April 2023.